HHS Public Access

Author manuscript

AJR Am J Roentgenol. Author manuscript; available in PMC 2022 August 26.

Published in final edited form as:

AJR Am J Roentgenol. 2022 July ; 219(1): 120–131. doi:10.2214/AJR.21.26777.

Paramagnetic Rim Lesions in Multiple Sclerosis: Comparison of Visualization at 1.5-T and 3-T MRI

Christopher C. Hemond, MD[1], **Daniel S. Reich, MD, PhD**[2], **Sathish K. Dundamadappa, MD**[3]

[1]Department of Neurology, University of Massachusetts Medical Center, 55 Lake Ave N, Worcester, MA 01655.

[2]Translational Neuroradiology Section, Division of Neuroimmunology and Neurovirology, National Institute of Neurological Disorders and Stroke, NIH, Bethesda, MD.

[3]Department of Radiology, University of Massachusetts Medical School, Worcester, MA.

Abstract

BACKGROUND.—Multiple sclerosis (MS) is characterized by both acute and chronic intrathecal inflammation. A subset of MS lesions show paramagnetic rims on susceptibility-weighted MRI sequences, reflecting iron accumulation in microglia. These paramagnetic rim lesions have been proposed as a marker of compartmentalized smoldering disease. Paramagnetic rim lesions have been shown at 7 T and, more recently, at 3 T. As susceptibility effects are weaker at lower field strength, it remains unclear if paramagnetic rim lesions are visible at 1.5 T.

OBJECTIVE.—The purpose of our study was to compare visualization of paramagnetic rim lesions using susceptibility-weighted imaging at 1.5-T and 3-T MRI in patients with MS.

METHODS.—This retrospective study included nine patients (five women, four men; mean age, 46.8 years) with MS who underwent both 1.5-T and 3-T MRI using a comparable susceptibility-weighted angiography (SWAN) sequence from the same manufacturer. Lesions measuring greater than 3 mm were annotated. Two reviewers independently assessed images at each field strength in separate sessions and classified the annotated lesions as isointense, diffusely paramagnetic, or paramagnetic rim lesions. Discrepancies were discussed at consensus sessions including a third reviewer. Agreement was assessed using kappa coefficients.

RESULTS.—Based on the 3-T consensus readings, 115 of 140 annotated lesions (82%) were isointense lesions, 16 (11%) were diffusely paramagnetic lesions, and nine (6%) were paramagnetic rim lesions; based on the 1.5-T consensus readings, 115 (82%) were isointense lesions, 14 (10%) were diffusely paramagnetic lesions, and 11 (8%) were paramagnetic rim lesions. The mean lesion diameter was 11.9 mm for paramagnetic rim lesions versus 6.4 mm for diffusely paramagnetic lesions ($p = .006$) and 7.8 mm for isointense lesions ($p = .003$). Interrater agreement for lesion classification as a paramagnetic rim lesion was substantial at 1.5 T ($\kappa = 0.65$)

Address correspondence to C. C. Hemond (Christopher.Hemond@umassmed.edu).

The authors declare that they have no disclosures relevant to the subject matter of this article.

The opinions and assertions contained herein are the private views of the authors and are not to be construed as official or as representing the views of the NIH.

An electronic supplement is available online at doi.org/10.2214/AJR.21.26777.

and 3 T (κ = 0.70). Agreement for paramagnetic rim lesions was also substantial between the consensus readings at the two field strengths (κ = 0.79).

CONCLUSION.—We show comparable identification of paramagnetic rim lesions at 1.5-T and 3-T MRI with substantial interrater agreement at both field strengths and substantial consensus agreement between the field strengths.

CLINICAL IMPACT.—Paramagnetic rim lesions may be an emerging marker of chronic neuroinflammation in MS. Their visibility at 1.5 T supports the translational potential of paramagnetic rim lesion identification to more widespread clinical settings, where 1.5-T scanners are prevalent.

Keywords

1.5 T; 3 T; chronic active lesion; filtered phase; iron rim lesion; multiple sclerosis; paramagnetic rim lesion; susceptibility-weighted imaging; T2*

Multiple sclerosis (MS) is typically characterized by recurrent episodes of immune-mediated CNS demyelination. Patients also commonly experience concurrent neurodegeneration, characterized indirectly as accelerated brain and spinal cord tissue loss compared with age-matched healthy populations. The mechanism of this neurodegenerative process is likely multifactorial and at least in part relates to chronic compartmentalized CNS inflammation [1, 2]. Although gadolinium enhancement serves as a reliable marker of acute (i.e., active) lesions, imaging detection of smoldering lesions remains challenging.

Susceptibility-weighted imaging has been shown to reveal novel characteristics of MS lesions, including the presence of a paramagnetic rim in a small subset of lesions [3, 4]. These lesions, described as “paramagnetic rim lesions” or as “iron rim lesions,” have been extensively characterized on 7-T MRI [5, 6]. MRI at 7 T is well suited for this investigation because of the field strength’s very high signal-to-noise ratio and sensitivity for detecting tissue susceptibility. Additional studies have reported that paramagnetic rim lesions correspond histopathologically with iron-enriched microglia and macrophages that express inflammatory markers [6–10]. Further recent studies have characterized paramagnetic rim lesions at 3-T MRI, reporting clinical associations of paramagnetic rim lesions with greater neurologic disability [11] and with lower normalized brain volumes, and have described a propensity toward expansion of the affected lesion by approximately 2% annually [12]. Given these properties, paramagnetic rim lesions are considered to represent chronic active lesions [4, 12–14], potentially serving as an important new marker of smoldering disease pathology in MS.

Susceptibility-induced signal loss is less prominent on MRI at lower field strengths. Thus, it may be anticipated that paramagnetic rim lesions would be less well visualized at 1.5 T than at 3 T, and indeed, effective visualization of paramagnetic rim lesions at 1.5 T has not been established. Because many MRI scanners used in clinical practice operate at 1.5 T, the widespread clinical translational utility of paramagnetic rim lesion depends to a large degree on whether these lesions can be reliably visualized at that field strength. To our knowledge, paramagnetic rim lesions have not been systematically compared between 1.5 T and 3 T in the same patients. Thus, in this study, we aimed to compare the visualization

of paramagnetic rim lesions using susceptibility-weighted imaging at 1.5-T and 3-T MRI in patients with MS.

Methods

Patients

This retrospective study was reviewed and approved by the University of Massachusetts ethics board. Data collection, storage, and access were in accordance with HIPAA. Patients were identified by search of institutional research databases of patients participating in various investigations of demyelinating disorders, most of which are ongoing prospective observational studies. Most patients had provided written informed consent as part of the prospective studies; the requirement for written informed consent for purposes of this investigation was waived for patients in one of three protocols.

The study included a convenience sample of patients who underwent MRI examinations with susceptibility-weighted imaging at both 1.5 T and 3 T. A search of the research databases identified 583 patients who had undergone MRI including susceptibility-weighted imaging at both field strengths as part of separate studies. Patients were then excluded for the following reasons: lack of MRI with susceptibility-weighted imaging protocol at both 1.5 T and 3 T (n = 568), diagnosis other than MS (n = 2), severe motion artifact on susceptibility-weighted imaging or FLAIR imaging (n = 1), no cerebral MS lesions on MRI measuring greater than 3 mm in maximal diameter (n = 2), and severe confluent lesion (n = 1). The diagnoses of MS had been established clinically according to 2017 McDonald criteria [15] by neurologists (non-authors) with subspecialty training in neuroimmunology. These exclusions resulted in a final study sample of nine patients (five women, four men; mean age, 46.8 ± 13.2 [SD] years). For the included patients, clinical data were extracted from the electronic medical record, including patient demographics, MS clinical phenotype, disease duration, treatment history, and neurologic disability as assessed using the expanded disability status scale [16].

MRI Acquisition

Patients underwent brain MRI at both 1.5 T and 3 T. Both examinations were performed using a susceptibility-weighted angiography (SWAN, GE Healthcare) sequence, which is based on a multiecho gradient-recalled echo (GRE) acquisition with a so-called “out-of-the-box” implementation (i.e., no modification of vendor-supplied parameters).

The 1.5-T examinations were performed using a Signa Artist scanner (GE Healthcare). The 1.5-T scanner was located in a hospital setting, and all patients were inpatients at the time of 1.5-T imaging. The 1.5-T protocol included a 3D SWAN sequence (TR, minimum value of ≈ 80 milliseconds; TE, 50 milliseconds; flip angle, 25°; echo-train length, 10; slice thickness, 3 mm; slice overlap, 1.5 mm; frequency phase, 320/256; reconstructed voxel size, 0.47 × 0.47 × 3 mm; acquisition time, 4 minutes 40 seconds) and a 2D axial fast spin-echo T2-weighted FLAIR sequence (TR/TE, 9000/140; inversion time, 2379 milliseconds; flip angle, 160°; slice thickness, 5 mm; interslice gap, 0.5 mm; frequency phase, 320/200; reconstructed voxel size, 0.94 × 0.94 × 5 mm; acquisition time, 3 minutes 46 seconds).

The 3-T examinations were performed using a Signa Pioneer scanner (GE Healthcare) that was located in an outpatient facility. The 3-T protocol included a 3D SWAN sequence (TR, minimum value of ≈ 42 milliseconds; TE, minimum value of ≈ 24 milliseconds; flip angle, 15°; echo-train length, 9; slice thickness, 3 mm; slice overlap, 1.5 mm; frequency/phase, 320/224; reconstructed voxel size, 0.47 × 0.47 × 3 mm; acquisition time, 2 minutes 27 seconds) and a 2D axial fast spin-echo T2-weighted FLAIR sequence (TR/TE, 9000/140; inversion time, 2250 milliseconds; flip angle, 160°; slice thickness, 4 mm; no interslice time, 3 minutes 42 seconds). 0.86 × 0.86 × 4 mm; acquisition time, 3 minutes 42 seconds).

The 3D SWAN and FLAIR sequences were performed without IV contrast material at both field strengths. The routine protocols at both field strengths also included contrast-enhanced T1-weighted images obtained after IV administration of gadolinium-based contrast material (gadoterate meglumine).

Image Analysis

The MRI acquisitions were reconstructed using manufacturer software on the scanner and exported in DICOM format. The susceptibility-weighted acquisition automatically underwent post-processing with a proprietary reconstruction algorithm to generate SWAN images (reflecting a combination of magnitude and phase data) and axial filtered-phase SWAN images (right-hand convention; paramagnetism indicated by hypointensity). The images were then converted to NIfTI format using dcm2niix software (version 1.0.20201102, Chris Rorden, Neuroimaging Tools & Resources Collaboratory) [17]. ITK-SNAP software (version 3.8, P. Yushkevich and G. Guido) was used to perform rigid coregistration of the filtered-phase SWAN and FLAIR images across both 1.5-T and 3-T acquisitions for each patient (6 *df*, mutual information criteria) [18].

A single investigator (C.C.H., a neurologist with subspecialty training in neuroimmunology and 5 years of postgraduate experience in neuroimaging of MS) reviewed the FLAIR images at both 1.5 T and 3 T. The investigator identified and marked all MS lesions identified at 3 T that measured greater than 3 mm in largest diameter; these labels were automatically propagated across the coregistered filtered-phase SWAN images at both field strengths [15]. Confluent lesion complexes were marked when the complexes could be visualized as distinctly identifiable lesions that were perpendicularly oriented.

At least 1 week after completion of the lesion marking, two investigators (C.C.H. and S.K.D., a neuroradiologist with 15 years of posttraining experience) independently reviewed images for each patient, aware of the lesions marked for evaluation. The 18 examinations (nine 1.5-T examinations and nine 3-T examinations) were reviewed in random order. While blinded to field strength for each examination, the raters reviewed the FLAIR and filtered-phase SWAN images. The images were reviewed using a standardized contrast level during these sessions without adjustment by the raters.

Using the FLAIR images, the raters classified the location of each marked lesion as follows: subcortical, deep white, or deep gray matter; periventricular area; leukocortical area; or infratentorial area. Using the filtered-phase SWAN images, the raters also classified each lesion as an isointense lesion, a diffusely paramagnetic (i.e., diffusely hypointense) lesion, or

a paramagnetic rim lesion (Fig. 1). Lesions were classified as paramagnetic rim lesions if exhibiting a distinct hypointense rim on filtered-phase SWAN images that involved at least 50% of the lesion's visualized rim on FLAIR images as well as an isointense (relative to normal-appearing white matter) central area. Raters also recorded whether susceptibility artifact grossly obscured lesions on filtered-phase SWAN images. One rater (S.K.D.) recorded lesion size as the largest axial lesion diameter on FLAIR images.

Six weeks later, one investigator (C.C.H.), blinded to the interpretations in the earlier sessions, repeated the analysis at 3 T to assess intrarater reliability. During this session, the investigator recorded two additional characteristics recorded for each lesion on filtered-phase SWAN images: the presence or absence of a hypointense "dot" or dots [11, 19, 20] (classified as present if one dot was observed) and the presence or absence of a centrally appearing vein or veins (if observed, classified as a single vein or multiple veins) [21].

After these review sessions, the results were unblinded, and lesions with interrater discrepancies were reviewed jointly by the two earlier investigators to establish consensus based on discussion for all features that both raters had assessed. The raters adjusted the image contrast freely during this consensus review. During the consensus review, the raters also reevaluated lesions classified as paramagnetic rim lesions at only one field strength even if both of the first two raters classified the lesion as not a paramagnetic rim lesion during the initial review. If uncertainty remained regarding potential lesion classification as a paramagnetic rim lesion, then an additional reviewer (D.S.R., a neurologist and neuroradiologist with 20 years of experience) was consulted for final determination of lesion classification. During the consensus sessions, one rater (C.C.H.) recorded qualitative reasons for discrepancies between raters and between field strengths as well as qualitative approaches for obtaining consensus, when applicable.

Lesions deemed to be grossly obscured by susceptibility artifact at either field strength at consensus interpretation were excluded from further analysis. In addition, after completion of all previously described analyses, one of the investigators (C.C.H.) reviewed postcontrast T1-weighted images while unblinded to other sequences and the clinical imaging reports to assess lesions for contrast enhancement. Lesions that showed enhancement on contrast-enhanced T1-weighted images at either field strength were also excluded from further analysis because these lesions may exhibit transient paramagnetic rims that do not necessarily indicate the presence of chronic neuroinflammation [22]. If a lesion was excluded from analysis due to susceptibility artifact or enhancement, other nonenhancing lesions in that patient remained in the analysis.

Statistical Analysis

Results were summarized using descriptive statistics. Cohen kappa coefficients for the two raters' classifications of lesions were calculated using both two unweighted categories (paramagnetic rim lesions vs non–paramagnetic rim lesions) and three unweighted categories (isointense lesions vs diffusely paramagnetic lesions vs paramagnetic rim lesions). Kappa coefficients were classified as follows [23]: poor agreement, less than 0.00; slight, 0.00–0.20; fair, 0.21–0.40; moderate, 0.41–0.60; substantial, 0.61–0.80; and almost perfect, 0.81–1.00. Consensus classifications were compared between field strengths. Mean

lesion diameters, based on the size measurements at 3 T, were compared between lesion types using two-tailed unpaired *t* tests. Lesion classifications were stratified by field strength and MS type. Sources of discrepancy were qualitatively summarized, and *p* values less than .05 were considered statistically significant. Statistical analyses were performed using an online calculator (Prism, GraphPad Software).

Results

Cohort Description

The characteristics of the nine patients in the study cohort are summarized in Table 1. Five patients had the relapsing remitting phenotype of MS, and four patients had the primary or secondary progressive phenotype of MS. The mean disease duration at the time of MRI was 12.6 ± 15.3 years. The 1.5-T MRI examination was performed first in six patients, and the 3-T MRI examination was performed first in three patients. The mean time difference between the 1.5-T and 3-T MRI scans was 7.3 ± 0.5 months (range, 2–18 months). Patients were receiving disease-modifying therapy at the time of MRI for six of the first examinations and seven of the second examinations. Contrast-enhanced imaging was performed for all nine examinations at 1.5 T and for six of the nine examinations at 3 T. For the three 3-T examinations performed without contrast material administration, one was performed before 1.5-T MRI, and two were performed after 1.5-T MRI.

Lesion Analysis

In the nine patients, a total of 146 MS lesions measuring greater than 3 mm were identified on FLAIR images. Six lesions were excluded from analysis due to being grossly obscured by susceptibility artifact ($n = 5$) or due to gadolinium enhancement ($n = 1$, observed at 1.5 T), resulting in inclusion of 140 lesions in the analysis. The locations of these 140 lesions were as follows: 54 (39%) were in subcortical, deep white, or deep gray matter; 51 (36%), periventricular; 32 (23%), leukocortical; and three (2%), infratentorial. Lesion characteristics on filtered-phase SWAN images included a hypointense dot or dots (3 T, $n = 10$ [7%]; 1.5 T, $n = 7$ [5%]), a single centrally appearing vein (3 T, $n = 29$ [21%]; 1.5 T, $n = 22$ [16%]), and multiple centrally appearing veins (3 T, $n = 9$ [6%]; 1.5 T, $n = 6$ [4%]).

Based on lesion categorization from the 3-T consensus readings of filtered-phase SWAN images, 115 (82%) lesions were isointense lesions, 16 (11%) were diffusely paramagnetic lesions, and nine (6%) were paramagnetic rim lesions. Based on the 1.5-T consensus readings, 115 (82%) lesions were isointense lesions, 14 (10%) were diffusely paramagnetic lesions, and 11 (8%) were paramagnetic rim lesions. A lesion classified as a paramagnetic rim lesion at both 1.5 T and 3 T is shown in Figure 2. The nine paramagnetic rim lesions at 3-T consensus were observed in five (56%) patients (four patients with a progressive phenotype and one with a relapsing remitting phenotype). Table 2 provides further details of the stratification of lesion classifications by field strength and MS type. The mean lesion diameter, as measured on FLAIR imaging, was significantly greater for paramagnetic rim lesions (11.9 mm) than isointense lesions (7.8 mm; $p = .003$) and diffusely paramagnetic lesions (6.4 mm; $p = .006$). Mean diameter was not significantly different between isointense lesions and diffusely paramagnetic lesions ($p = .13$).

Inter- and Intrarater Agreement

Inter- and intrarater agreement for the classification of lesions as paramagnetic rim lesion versus non–paramagnetic rim lesion at both 1.5 T and 3 T was substantial or almost perfect (Table 3). For example, interrater agreement, expressed as kappa, was 0.65 at 1.5 T and 0.70 at 3 T. When assessing agreement among three categories (isointense lesion, diffusely paramagnetic lesion, paramagnetic rim lesion), inter- and intrarater agreement remained substantial or almost perfect at both field strengths (i.e., $\kappa = 0.69$ at 1.5 T and 0.66 at 3 T; Table 4). Percent agreements in the various assessments of rater agreement ranged from 89% to 98%.

Assessment of Intra- and Interrater Discordances

The classification of lesions as a paramagnetic rim lesion was discordant between the initial two reviewers for 10 lesions (six discrepant classifications at 1.5 T; four discrepant classifications at 3 T). The reasons for interrater discrepancy identified at consensus discussion included (multiple reasons possible if individual cases): vascular complexity (contributed in 6/10 lesions), poor signal or contrast (5/10 lesions), small lesion size (2/10 lesions), and potential distortion from artifact-susceptible location (e.g., proximity to bone-tissue or air-tissue interface) (2/10 lesions). The classification of lesions as a paramagnetic rim lesion was discordant on the intrarater analysis at 3 T for five lesions, three of which were not identified by either rater on the earlier 3-T interpretation session. The reasons for intrarater discrepancy included the following: faint signal in the rim (3/5), heterogeneous partial rim (1/5), and vascular complexity (1/5).

The classification of lesions as isointense versus diffusely heterogeneous was discordant between the initial two reviewers for 19 lesions (eight discrepant classifications at 1.5 T; 11 discrepant classifications at 3 T). At consensus discussion, all 19 discrepancies were attributed at least in part to heterogeneous paramagnetic content within the lesion. This heterogeneity was attributed to the presence of vessels in four lesions and to possible distortion near an artifact-susceptible region in two lesions and was of an unknown cause in 13 lesions. To attain consensus, the raters applied a more stringent definition of a diffusely paramagnetic lesion—namely, that at least 75% of the lesion's area showed paramagnetic signal. Figure S1 (available in the online supplement) shows an example of a lesion with discordant classification between raters as isointense or diffusely heterogeneous; in that lesion (Fig. S1), the heterogeneous paramagnetic content was in part due to paramagnetic signal within the optic radiations.

Assessment of Discordances Between 1.5 T and 3 T

Agreement between 1.5 T and 3 T in terms of consensus lesion classifications, expressed as kappa, was 0.79 for classification as a paramagnetic rim lesion versus a non–paramagnetic rim lesion and was 0.70 for classification as an isointense lesion, diffusely paramagnetic lesion, or paramagnetic rim lesion. Table 5 provides a cross-tabulation of consensus lesion classifications at 1.5 T and 3 T. One lesion was classified as a paramagnetic rim lesion at 3 T but not at 1.5 T; three lesions were classified as paramagnetic rim lesions at 1.5 T but not at 3 T. At consensus discussion, the lesion classified as a paramagnetic rim lesion only at 3 T was thought to relate to a combination of an incomplete rim and the lesion

being part of a confluent complex (Fig. 3). This patient underwent 3-T MRI 14 months after 1.5-T MRI. The reasons for classifying lesions as paramagnetic rim lesions only at 1.5 T included the following: circular-appearing vessel configuration leading to possible erroneous classification at 1.5 T (two lesions, with intervals between MRI examinations of 5 and 18 months) (Fig. S2, available in the online supplement) and possible lesion evolution over time (one lesion; interval between examinations of 18 months).

During the consensus review, two additional lesions were classified as a paramagnetic rim lesion despite neither rater classifying the lesion as a paramagnetic rim lesion at initial review. These classifications occurred once the lesions were reevaluated in conjunction with the third rater and with awareness that the lesions had been classified as paramagnetic rim lesions at the other field strength. One lesion, with an MRI interval of 2 months, had initially been classified as a paramagnetic rim lesion only at 3 T but on consensus review was observed to exhibit a faint paramagnetic rim at 1.5 T as well (Fig. S3A, available in the online supplement). The other lesion, with an MRI interval of 14 months, had initially been classified as a paramagnetic rim lesion only at 1.5 T but on consensus review was observed to exhibit a paramagnetic rim that had been obscured by lesion heterogeneity and susceptibility artifact from prominent vasculature (Fig. S3B).

Discussion

The paramagnetic rim lesion may be an important emerging MRI marker of ongoing low-grade intrathecal inflammation in MS. In this study, we show comparable identification of paramagnetic rim lesions at 1.5-T and 3-T MRI with substantial interrater agreement at both field strengths and substantial consensus agreement between the field strengths. This comparable identification between field strengths is an unexpected finding and supports the feasibility of adoption of a paramagnetic rim lesion as a potential marker on widely available 1.5-T MRI platforms, while substantiating the need for establishment of clear criteria for paramagnetic rim lesion discrimination.

We identified paramagnetic rim lesions using the 3D SWAN sequence. Other manufacturers offer similar susceptibility-weighted sequences, including SWI from Siemens Healthineers and SWIp from Philips Healthcare, which also use multiecho GRE acquisition to derive filtered-phase SWAN images with high signal-to-noise ratio. Our unmodified implementation of the SWAN sequence yielded natively high resolution in the axial plane (reconstructed 0.47 × 0.47 mm) but relatively thick slices of 3 mm, producing anisotropic voxels with 1.5-mm overlap. Our observed interrater agreement for paramagnetic rim lesions at 3 T is similar to prior studies. One group found an interrater agreement, measured as intraclass correlation coefficient, of 0.84 [20] using the SWI sequence at 3 T with 0.65 × 0.65 × 3.0 mm voxels. Additionally, Absinta et al. [4] reported a kappa coefficient of 0.86 at 3 T, and Maggi et al. [24] reported a kappa coefficient of 0.79 in a multicenter cohort at 3 T using an echoplanar imaging (EPI)-based filtered-phase T2*-weighted protocol. We observed a kappa coefficient of 0.79 for the consensus classification of lesions as paramagnetic rim lesions between 1.5 T and 3 T, which is similar to a kappa coefficient of 0.78 between 3 T and 7 T reported by Absinta et al. [4]. In general, differences in lesion categorization between field strengths could relate to acquisition parameters (EPI vs GRE),

use of isotropic versus anisotropic voxels, voxel resolution, lesion selection method, criteria for paramagnetic rim lesion identification, and reduced susceptibility contrast at lower field strengths.

Our work is not the first to identify paramagnetic rim lesions at 1.5 T; an earlier study described paramagnetic rims in 5% (7/141) of MS lesions in a group of 14 patients scanned at 1.5 T using a voxel size of 1.0 × 1.0 × 2.0 mm [3], which is comparable to our classification of 8% (11/140) of lesions as paramagnetic rim lesions at 1.5 T. Our classification of 6% of lesions as paramagnetic rim lesions at 3 T also falls within the range of previously reported frequencies at 3 T, from 4.6% (28/611 lesions in 66 patients with early MS; GRE-SWI at 1 × 1 × 1 mm) [11] to 19.9% (127/636 lesions in 112 patients with clinically isolated syndrome; GRE-SWI at 0.65 × 0.65 × 3.0 mm) [20].

The reported frequency of paramagnetic rim lesions at 7 T has varied as well, including frequencies of 4.2% (8/191 lesions in nine patients; SWI at 0.23 × 0.23 × 2.0 mm) [5], 14% (55/396 lesions in 17 patients; GRE-T2* phase imaging at 0.2 × 0.2 × 1 mm) [6], 15% (28/183 lesions in 10 patients; SWI at 0.3 × 0.3 × 1.2 mm) [14], and 54% in the study by Dal-Bianco et al. [14] when excluding lesions with confluent characteristics. This variation in frequency across studies at a single field strength likely relates to a range of technical and qualitative factors, including differences in the sequences used.

The lesions that we describe as paramagnetic rim lesions have also been described as iron rim lesions or chronic active lesions. Whereas the term “paramagnetic rim lesion” is a purely descriptive term, these alternate terms connote these lesions’ likely composition and functional properties. However, phase contrast, as shown on the filtered-phase SWAN images, reflects more than just the presence of iron but, rather, is affected by a combination of local tissue susceptibility properties that can include loss of diamagnetic myelin, changes in paramagnetic deoxyhemoglobin, and the presence of free radicals [22]. Although likely dominated by the superparamagnetic effects of iron, phase images cannot reliably quantify iron concentration [25] because phase signal also depends on field strength and TE. Indeed, by doubling the TE at a lower field strength, the phase can remain constant just as it would at a higher field strength albeit at the expense of reduced signal [3].

Although interrater agreement was substantial, discrepancies were observed at both field strengths. The most common reasons for discordant interrater classifications of paramagnetic rim lesions included vascular complexity and poor signal or contrast. Although not assessed by our study, part of a paramagnetic rim lesion rim may be particularly prone to be mistaken for a prominent vessel in regions with a high density of medullary veins, such as in the periventricular area; the paramagnetic rim lesion rim may also be difficult to detect in areas that are particularly sensitive to bulk susceptibility artifacts, such as the orbitofrontal cortex and anterior temporal lobes. Additional challenges in paramagnetic rim lesion identification included confluent lesions and paramagnetic rim lesions with partial rims. Finally, intrarater agreement was decreased by variable detection of faint lesions, suggesting a limitation from the rater’s subjective (and potentially variable) threshold for deeming a lesion to be a paramagnetic rim lesion. These sources of ambiguity in paramagnetic rim lesion classification convey the need for optimized consensus

definitions and protocols. Absinta et al. [4] provided similar observations for inter- and intrarater agreement in paramagnetic rim lesion classification and recommended dedicated neuroimaging training before assessment of this imaging feature.

We did not observe detection of a greater total number of paramagnetic rim lesions at 3 T than at 1.5 T, as might have been anticipated. However, consensus discussion suggested that the paramagnetic rim lesion visualized only at 3 T was likely a true paramagnetic rim lesion that was missed at 1.5 T due to decreased signal. On the other hand, paramagnetic rim lesions identified only at 1.5 T were thought to likely represent false-positive paramagnetic rim lesions at 1.5 T related to vascular complexity in two cases and to temporal evolution of the lesion in a third case. Alternatively, although paramagnetic rim lesions have been previously shown to be stable over a period of months to years, it is possible that the variation between field strengths may have been related in part to dynamic evolution of lesions. This potential evolution of paramagnetic rim lesions is an area of ongoing research that may be particularly relevant for the patient in our study with an interval between MRI examinations of 18 months (patient 6 in Table 1).

Another challenge inherent to the SWAN sequence used in the current study is its anisotropic voxel size (reconstructed 0.47 × 0.47 × 3 mm), which may limit visualization of the entire lesion in the axial plane. The relatively thick slices can contribute to false-negatives by capturing only the peripheral edge of a small paramagnetic rim lesion, resulting in a heterogeneous appearance without a distinct rim and ultimate classification as a diffusely paramagnetic lesion. This situation may be addressed through a clear a priori definition for a diffusely paramagnetic lesion in addition to a definition for a paramagnetic rim lesion. In the post hoc consensus, we chose greater than 75% paramagnetic content as a threshold for diffusely paramagnetic lesions. Although not considered in the present investigation, an alternative lesion classification of heterogeneously paramagnetic may have been simpler than the classification of diffusely paramagnetic and may have reduced subjectivity. Lesion classification as diffusely paramagnetic should ultimately be grounded on biologic significance, highlighting the need for additional research exploring histologic-imaging classification of variable paramagnetic lesion content.

The clinical implications of this study remain preliminary. Evidence for the prognostic and diagnostic utility of the MRI finding of paramagnetic rim lesions are emerging and currently lack widespread replication, especially on different MRI platforms and field strengths. Although we did not systematically assess the time required to evaluate and categorize lesions, from a practical standpoint, we estimate that interpreting the susceptibility features of each MS lesion would add several minutes of radiologist time for examinations with multiple lesions.

The limitations of this study include the small sample size and possible selection bias. Examinations were performed using a susceptibility-weighted sequence from a single vendor; results may differ using other sequences for paramagnetic rim lesion assessment. In addition, patients were inpatients at the time of 1.5-T MRI and thus were likely experiencing acute neurologic issues. This risk is partially mitigated by the exclusion from the analysis of the one gadolinium-enhancing lesion. Another limitation is the interval of 2–

18 months between the two MRI examinations in each patient. Although most paramagnetic rim lesions have been shown to be stable on that time scale [6, 9], a component of dynamic susceptibility might have influenced the comparisons between field strengths, as previously noted. Indeed, recent work has shown that paramagnetic rim lesions often fade over the course of many years [9, 13]. We also did not explore a possible association of disease-modifying treatments and the appearance of paramagnetic rim lesions. Finally, an external reference standard for the presence of paramagnetic rim lesions was not available. Thus, although we compared paramagnetic rim lesion classification between field strengths, sensitivity and specificity cannot be determined.

Conclusion

In patients with MS evaluated by MRI using susceptibility-weighted acquisitions, paramagnetic rim lesions are visible on 1.5-T MRI, and detection of these lesions on 1.5-T MRI compares favorably to 3-T MRI. These results support the translational potential of paramagnetic rim lesion identification to more widespread clinical settings where 1.5-T scanners are prevalent. The findings have additional relevance for large phase III clinical trials, which are increasingly enrolling participants from low- and middle-income countries that may have older lower-field-strength MRI hardware. Although the paramagnetic rim lesions identified in this study are likely to be similar to those previously described at 7 T using other susceptibility-weighted methods, further histopathologic and clinical validation is needed to determine the biologic relevance of the lesions identified using our protocol at lower field strengths.

Supplementary Material

Refer to Web version on PubMed Central for supplementary material.

Acknowledgments

We thank our colleagues including Carolina Ionete, Roberto Bomprezzi, Idanis Berrios-Morales, and Raffaella Umeton as well as Celia Gomes-McGillivray at the University of Massachusetts for contributions to patient recruitment in ongoing longitudinal observational studies.

Supported by the National Center for Advancing Translational Sciences, NIH (grant KL2TR001454); the National Multiple Sclerosis Society (grant to C. C. Hemond); and the National Institute of Neurological Disorders and Stroke, NIH (grant to D. S. Reich).

References

1. Reich DS, Lucchinetti CF, Calabresi PA. Multiple sclerosis. N Engl J Med 2018; 378:169–180 [PubMed: 29320652]
2. Louapre C, Lubetzki C. Neurodegeneration in multiple sclerosis is a process separate from inflammation: yes. Mult Scler 2015; 21:1626–1628 [PubMed: 26515289]
3. Haacke EM, Makki M, Ge Y, et al. Characterizing iron deposition in multiple sclerosis lesions using susceptibility weighted imaging. J Magn Reson Imaging 2009; 29:537–544 [PubMed: 19243035]
4. Absinta M, Sati P, Fechner A, Schindler MK, Nair G, Reich DS. Identification of chronic active multiple sclerosis lesions on 3T MRI. AJNR 2018; 39:1233–1238 [PubMed: 29724768]
5. Chawla S, Kister I, Sinnecker T, et al. Longitudinal study of multiple sclerosis lesions using ultra-high field (7T) multiparametric MR imaging. PLoS One 2018; 13:e0202918 [PubMed: 30212476]

6. Absinta M, Sati P, Schindler M, et al. Persistent 7-Tesla phase rim predicts poor outcome in new multiple sclerosis patient lesions. J Clin Invest 2016; 126:2597–2609 [PubMed: 27270171]
7. Bagnato F, Hametner S, Yao B, et al. Tracking iron in multiple sclerosis: a combined imaging and histopathological study at 7 Tesla. Brain 2011; 134:3602–3615 [PubMed: 22171355]
8. Mehta V, Pei W, Yang G, et al. Iron is a sensitive biomarker for inflammation in multiple sclerosis lesions. PLoS One 2013; 8:e57573 [PubMed: 23516409]
9. Dal-Bianco A, Grabner G, Kronnerwetter C, et al. Long-term evolution of multiple sclerosis iron rim lesions in 7 T MRI. Brain 2021; 144:833–847 [PubMed: 33484118]
10. Gillen KM, Mubarak M, Park C, et al. QSM is an imaging biomarker for chronic glial activation in multiple sclerosis lesions. Ann Clin Transl Neurol 2021; 8:877–886 [PubMed: 33704933]
11. Blindenbacher N, Brunner E, Asseyer S, et al. Evaluation of the 'ring sign' and the 'core sign' as a magnetic resonance imaging marker of disease activity and progression in clinically isolated syndrome and early multiple sclerosis. Mult Scler J Exp Transl Clin 2020; 6:2055217320915480 [PubMed: 32284875]
12. Absinta M, Sati P, Masuzzo F, et al. Association of chronic active multiple sclerosis lesions with disability in vivo. JAMA Neurol 2019; 76:1474–1483 [PubMed: 31403674]
13. Absinta M, Maric D, Gharagozloo M, et al. A lymphocyte-microglia-astrocyte axis in chronic active multiple sclerosis. Nature 2021; 597:709–714 [PubMed: 34497421]
14. Dal-Bianco A, Grabner G, Kronnerwetter C, et al. Slow expansion of multiple sclerosis iron rim lesions: pathology and 7 T magnetic resonance imaging. Acta Neuropathol 2017; 133:25–42 [PubMed: 27796537]
15. Thompson AJ, Banwell BL, Barkhof F, et al. Diagnosis of multiple sclerosis: 2017 revisions of the McDonald criteria. Lancet Neurol 2018; 17:162–173 [PubMed: 29275977]
16. Kurtzke JF. Rating neurologic impairment in multiple sclerosis: an expanded disability status scale (EDSS). Neurology 1983; 33:1444–1452 [PubMed: 6685237]
17. Li X, Morgan PS, Ashburner J, Smith J, Rorden C. The first step for neuroimaging data analysis: DICOM to NIfTI conversion. J Neurosci Methods 2016; 264:47–56 [PubMed: 26945974]
18. Yushkevich PA, Piven J, Hazlett HC, et al. User-guided 3D active contour segmentation of anatomical structures: significantly improved efficiency and reliability. Neuroimage 2006; 31:1116–1128 [PubMed: 16545965]
19. Hagemeier J, Heininen-Brown M, Poloni GU, et al. Iron deposition in multiple sclerosis lesions measured by susceptibility-weighted imaging filtered-phase: a case control study. J Magn Reson Imaging 2012; 36:73–83 [PubMed: 22407571]
20. Clarke MA, Pareto D, Pessini-Ferreira L, et al. Value of 3T susceptibility-weighted imaging in the diagnosis of multiple sclerosis. AJNR 2020; 41:1001–1008 [PubMed: 32439639]
21. Sati P, Oh J, Constable RT, et al. ; NAIMS Cooperative. The central vein sign and its clinical evaluation for the diagnosis of multiple sclerosis: a consensus statement from the North American Imaging in Multiple Sclerosis Cooperative. Nat Rev Neurol 2016; 12:714–722 [PubMed: 27834394]
22. Absinta M, Sati P, Gaitán MI, et al. Seven-Tesla phase imaging of acute multiple sclerosis lesions: a new window into the inflammatory process. Ann Neurol 2013; 74:669–678 [PubMed: 23813441]
23. Landis JR, Koch GG. The measurement of observer agreement for categorical data. Biometrics 1977; 33:159–174 [PubMed: 843571]
24. Maggi P, Sati P, Nair G, et al. Paramagnetic rim lesions are specific to multiple sclerosis: an international multicenter 3T MRI study. Ann Neurol 2020; 88:1034–1042 [PubMed: 32799417]
25. Yao B, Li T-Q, van Gelderen P, Shmueli K, de Zwart JA, Duyn JH. Susceptibility contrast in high field MRI of human brain as a function of tissue iron content. Neuroimage 2009; 44:1259–1266 [PubMed: 19027861]

HIGHLIGHTS

Key Finding

- Of 140 lesions in nine patients with MS, 11 lesions at 1.5 T and nine lesions at 3 T were classified as paramagnetic rim lesions. Agreement for paramagnetic rim lesions was substantial at 1.5 T (κ = 0.65) and 3 T (κ = 0.70) and between consensus readings at the two field strengths (κ = 0.79).

Importance

- This study represents an important step in establishing the translational potential of paramagnetic rim lesions at 1.5 T as a marker of chronic CNS inflammation in MS.

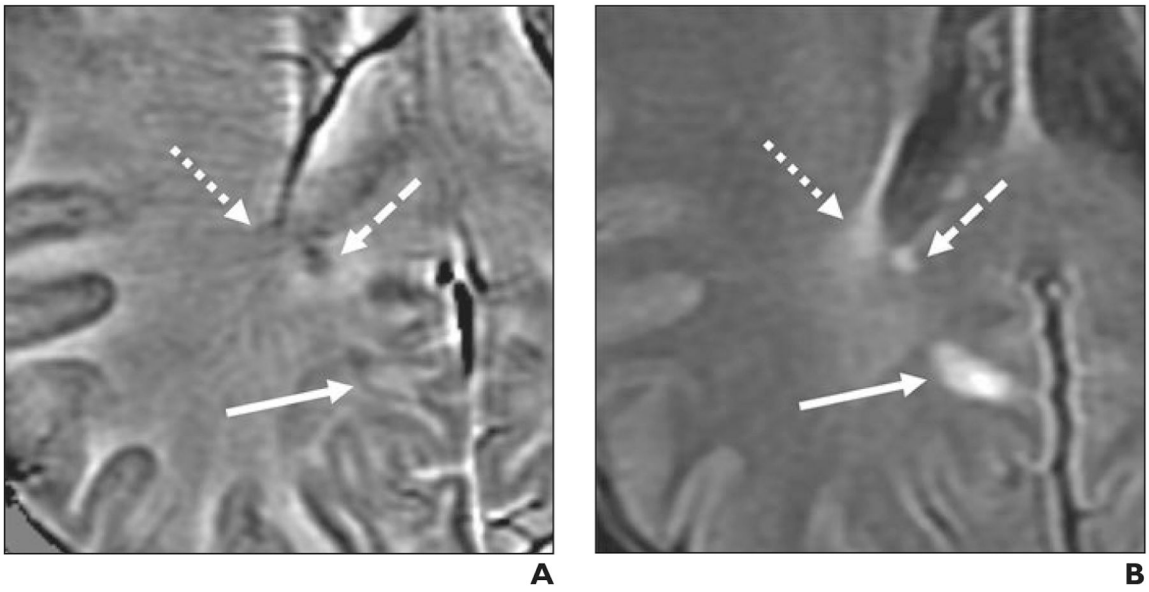

Fig. 1—.

Examples of three lesion classifications based on paramagnetic characteristics.

A and **B,** Axial filtered-phase susceptibility-weighted angiography (SWAN, GE Healthcare) (**A**) and FLAIR (**B**) images obtained at 3-T MRI in 49-year-old man (patient 1 in Table 1) with relapsing remitting multiple sclerosis show three lesion classifications in this study: isointense lesion (*dotted arrows*), which is flanked by prominent medullary veins; diffusely paramagnetic lesion (*dashed arrows*); and paramagnetic rim lesion with partial rim (*solid arrows*).

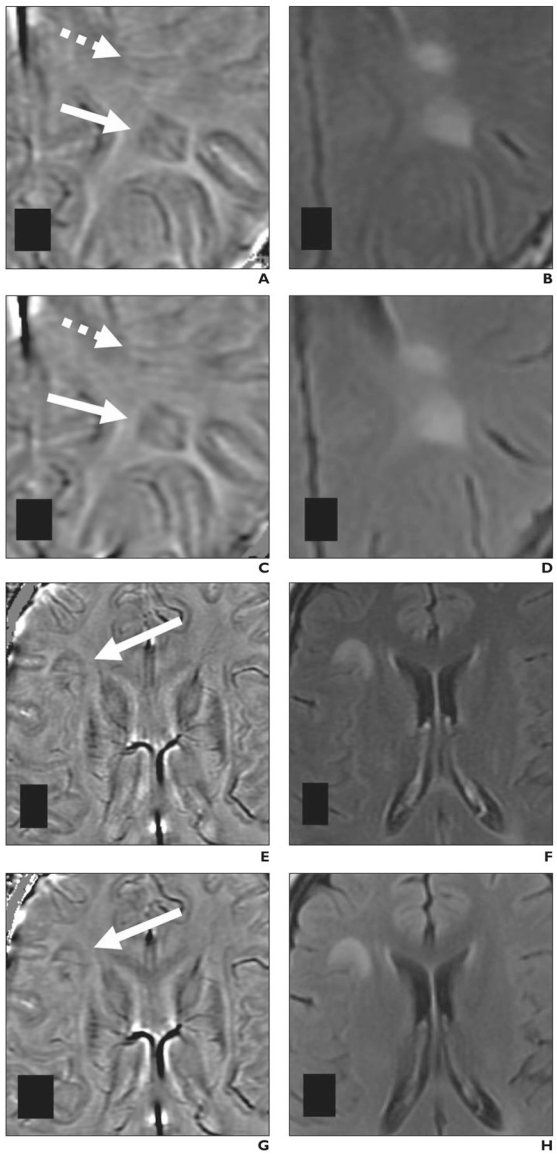

Fig. 2—.

Paramagnetic rim lesions detected at 1.5-T and 3-T MRI in 28-year-old woman (patient 3 in Table 1) with multiple sclerosis. Both MRI examinations included susceptibility-weighted angiography (SWAN, GE Healthcare) sequence; 1.5-T MRI was performed 2 months before 3-T MRI.

A–D, Paramagnetic rim lesion 1 (*solid arrows*, **A** and **C**) is shown on 1.5-T (**A** and **B**) and 3-T (**C** and **D**) axial filtered-phase SWAN (**A** and **C**) and FLAIR (**B** and **D**) images. Lesion 1 shows central vein at both field strengths. Dashed arrows in **A** and **C** depict FLAIR lesion with isointense signal on filtered-phase SWAN images; in this latter lesion, orientation of medullary veins on 1.5-T image (**A**) could result in this lesion being misinterpreted as paramagnetic rim lesion. **E–H,** Paramagnetic rim lesion 2 (*arrows*, **E** and **G**) is shown on 1.5-T (**E** and **F**) and 3-T (**G** and **H**) axial filtered-phase SWAN (**E** and **G**) and FLAIR (**F** and **H**) images.

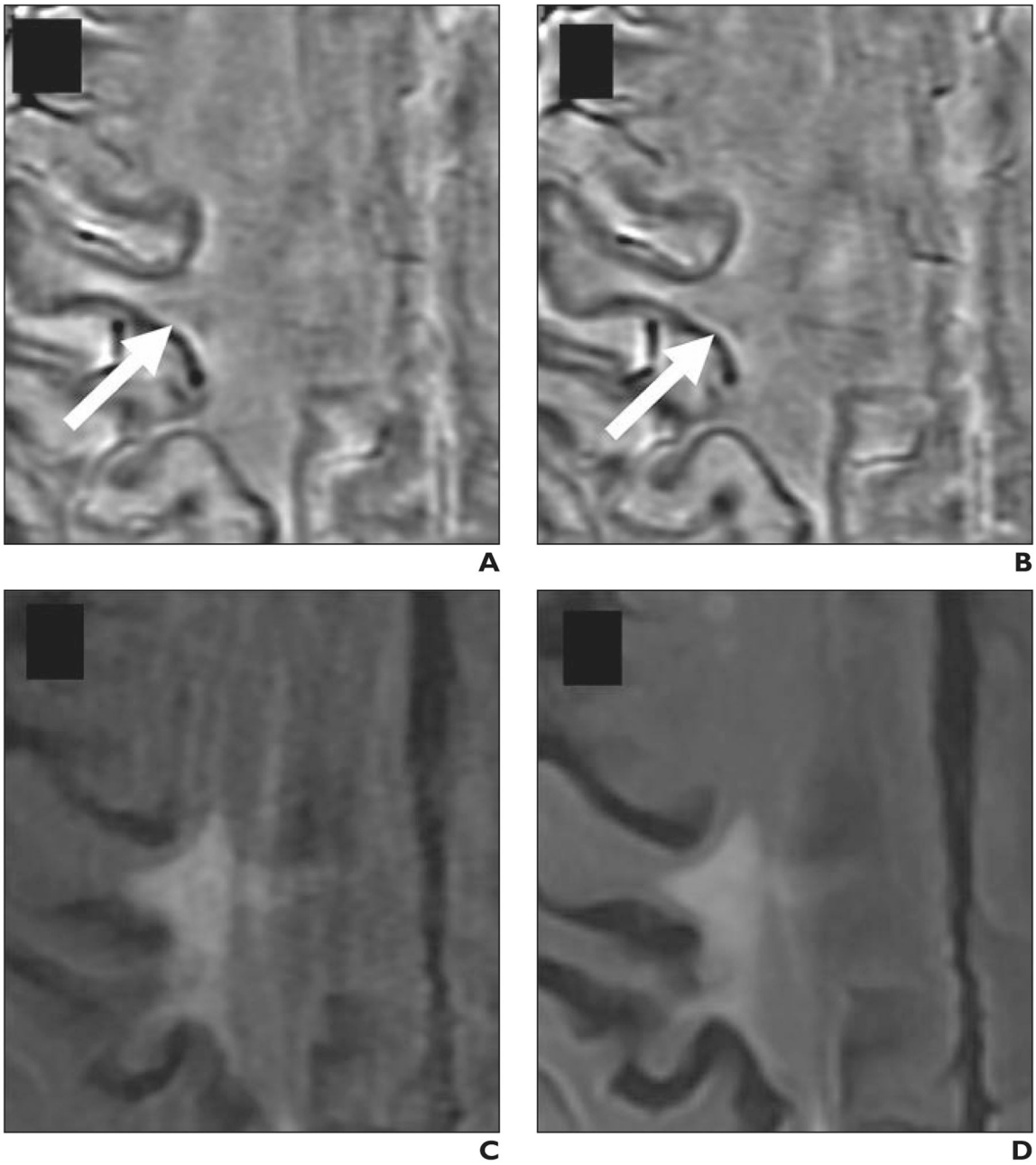

Fig. 3—.

Paramagnetic rim lesion that is more visible at 3 T compared with at 1.5 T. Axial filtered-phase susceptibility-weighted angiography (SWAN, GE Healthcare) and FLAIR images in 64-year-old man (patient 4 in Table 1) with multiple sclerosis show lesion with discordant classification between field strengths.

A and **B,** Lesion (*arrows*) was classified as isointense lesion on 1.5-T filtered-phase SWAN (**A**) and 1.5-T FLAIR (**B**) images. Features contributing to lesion not being classified as paramagnetic rim lesion at 1.5 T include incomplete rim and FLAIR lesion being part of confluent complex.

C and **D,** Lesion was classified as paramagnetic rim lesion on 3-T filtered-phase SWAN (**C**) and 3-T FLAIR (**D**) images.

TABLE 1:

Cohort Description and Clinical Characteristics

Patient No.	MS Type	Age (y)	Sex	EDSS Score	MS Duration (y)	DMT at Time of First MRI	DMT at Time of Second MRI	Interval Between First MRI and Second MRI (mo)	No. of Lesions > 3 mm	No. of Paramagnetic Rim Lesions[a]
1	RR	49	M	1.5	< 1	None	None	2	10	2
2	RR	33	F	1.5	7	RTX	RTX	5	20	0
3	PP	28	F	6	1	None	OCZ	2	6	3
4	SP	64	M	4	30	GA	TER	14	23	2
5	RR	37	M	1.5	< 1	GA	GA	6	3	0
6	SP	56	M	6.5	15	None	None	18	28	1
7	RR	41	F	1.5	6	OCZ	OCZ	3	7	0
8	RR	49	F	3	11	GA	TER	5	19	0
9	SP	64	F	6.5	45	ALZ	ALZ	11	24	1

Note—MS = multiple sclerosis, EDSS = expanded disability status scale (a method of quantifying disability in MS and monitoring changes in the level of disability over time), DMT = disease-modifying therapy, RR = relapsing remitting, RTX = rituximab, PP = primary progressive, OCZ = ocrelizumab, SP = secondary progressive, GA = glatiramer acetate, TER = teriflunomide, ALZ = alemtuzumab.

[a]Values are from 3-T MRI consensus reading.

AJR Am J Roentgenol. Author manuscript; available in PMC 2022 August 26.

TABLE 2:

Distribution of Consensus Lesion Classifications Stratified by Field Strength and MS Type

Field Strength and MS Type	No. of Patients	No. of Isointense Lesions	No. of Diffusely Paramagnetic Lesions	No. of Paramagnetic Rim Lesions
1.5 T				
RR	5	47	9	3
SP	3	66	4	5
PP	1	2	1	3
3 T				
RR	5	44	13	2
SP	3	69	2	4
PP	1	2	1	3

Note—MS = multiple sclerosis, RR = relapsing remitting, SP = secondary progressive, PP = primary progressive.

AJR Am J Roentgenol. Author manuscript; available in PMC 2022 August 26.

TABLE 3:

Inter- and Intrarater Agreement for Classification of Lesions as Paramagnetic Rim Lesions Versus Non–Paramagnetic Rim Lesions on Filtered-Phase SWAN[a] Images

Assessment	Percent Agreement	Cohen Kappa (± SE)	Agreement[b]
1.5 T			
Interrater (two raters)	96 (134/140)	0.65 ± 0.13	Substantial
Rater 1 vs 1.5-T consensus	97 (136/140)	0.76 ± 0.11	Substantial
Rater 2 vs 1.5-T consensus	97 (136/140)	0.80 ± 0.09	Substantial
3 T			
Intrarater (one rater)	96 (135/140)	0.72 ± 0.12	Substantial
Interrater (two raters)	97 (136/140)	0.70 ± 0.14	Substantial
Rater 1 vs 3-T consensus	96 (135/140)	0.65 ± 0.14	Substantial
Rater 2 vs 3-T consensus	98 (137/140)	0.81 ± 0.11	Almost perfect
1.5 T vs 3 T			
1.5-T consensus vs 3-T consensus	97 (136/140)	0.79 ± 0.10	Substantial

Note—Values in parentheses are raw data (number of lesions) used to calculate percent agreement. SWAN = susceptibility-weighted angiography, SE = standard error.

[a]GE Healthcare.

[b]Kappa coefficients were classified as follows [23]: poor agreement, less than 0.00; slight, 0.00–0.20; fair, 0.21–0.40; moderate, 0.41–0.60; substantial, 0.61–0.80; and almost perfect, 0.81–1.00.

TABLE 4:

Inter- and Intrarater Agreement for Classification of Lesions Among Three Categories of Paramagnetic Features[a] on Filtered-Phase SWAN[b] Images

Assessment	Percent Agreement	Cohen Kappa (± SE)	Agreement[c]
1.5 T			
Interrater (two raters)	90 (126/140)	0.69 ± 0.07	Substantial
Rater 1 vs 1.5-T consensus	94 (131/140)	0.80 ± 0.06	Substantial
Rater 2 vs 1.5-T consensus	96 (134/140)	0.86 ± 0.05	Almost perfect
3 T			
Intrarater (one rater)	91 (127/140)	0.73 ± 0.07	Substantial
Interrater (two raters)	89 (125/140)	0.66 ± 0.08	Substantial
Rater 1 vs 3-T consensus	94 (131/140)	0.78 ± 0.07	Substantial
Rater 2 vs 3-T consensus	94 (131/140)	0.80 ± 0.06	Substantial
1.5 T vs 3 T			
1.5-T consensus vs 3-T consensus	89 (127/140)	0.70 ± 0.08	Substantial

Note—Values in parentheses are raw data (number of lesions) used to calculate percent agreement. SWAN = susceptibility-weighted angiography, SE = standard error.

[a]The three categories of paramagnetic features are isointense, diffusely paramagnetic, and paramagnetic rim lesions.

[b]GE Healthcare.

[c]Kappa coefficients were classified as follows [23]: poor agreement, less than 0.00; slight, 0.00–0.20; fair, 0.21–0.40; moderate, 0.41–0.60; substantial, 0.61–0.80; and almost perfect, 0.81–1.00.

TABLE 5:

Cross-Tabulation of Consensus Lesion Categorizations at 1.5-T MRI and 3-T MRI

1.5 T	3 T		
	No. of Isointense Lesions	**No. of Diffusely Paramagnetic Lesions**	**No. of Paramagnetic Rim Lesions**
No. of isointense lesions	109	5	1
No. of diffusely paramagnetic lesions	4	10	0
No. of paramagnetic rim lesions	2	1	8